

# Quantum Mechanics of One-Dimensional Trapped Tonks Gases

M. D. Girardeau\* and E. M. Wright†

*Optical Sciences Center*

*University of Arizona*

*Tucson, AZ 85721, USA*

(October 24, 2018)

## Abstract

Several experimental groups are currently working towards realizing quasi-one-dimensional (1D) atom de Broglie waveguides and loading them with ultracold atoms. The dynamics becomes truly 1D in a regime (Tonks gas) of low temperatures and densities, and large positive scattering lengths for which the transverse mode becomes frozen, in which case the many-body Schrödinger dynamics becomes exactly soluble via a Fermi-Bose mapping theorem. In this paper we review our recent work on the exact ground state and quantum dynamics of 1D Tonks gases and assess the possibility of approaching the Tonks regime using Bessel beam optical dipole traps.

---

\*Email: girardeau@optics.arizona.edu

†Email: Ewan.Wright@optics.arizona.edu

## I. INTRODUCTION

Recent advances in atom de Broglie waveguide technology [1–5] and its potential applicability to atom interferometry [6] and integrated atom optics [3,7] create a need for accurate theoretical modelling of such systems in the low temperature, tight waveguide regime where transverse excitations are frozen out and the quantum dynamics becomes essentially one-dimensional (1D) (Tonks-gas limit). It has been shown by Olshanii [8], and also recently by Petrov et al. [9], that at sufficiently low temperatures and densities, high transverse frequencies  $\omega_T$ , and large positive scattering length, where thermal and longitudinal zero-point energies are small compared with  $\hbar\omega_T$ , a Bose-Einstein condensate (BEC) in a thin cigar-shaped trap has dynamics which reduce to those of a 1D gas of hard core, or impenetrable, point bosons. This is a model for which the exact many-body energy eigensolutions were found in 1960 using an exact mapping from the Hilbert space of energy eigenstates of an *ideal* gas of spinless fermions to that of many-body eigenstates of hard core, and therefore *strongly interacting*, bosons [10,11]. In this limit there are strong short-range pair correlations which are omitted in the Gross-Pitaevskii (GP) approximation, which assumes that all  $N$  bosons occupy the same orbital (complete BEC, condensed fraction unity). In the absence of a trap potential it is known [12] that the occupation of the lowest orbital is of order  $\sqrt{N}$  where  $N$  is the total number of atoms, in contrast to  $N$  for the ideal Bose gas as well as the GP approximation. Nevertheless, this system exhibits some BEC-like behavior such as Talbot recurrences following an optical lattice pulse [13] and dark soliton-like behavior in response to a phase-imprinting pulse [14].

The case of harmonically trapped, hard core bosons in 1D is more relevant to recent atom waveguide experiments [15]. The spatial profile of the single-particle density is expressible in closed form, and has recently been shown [16] to be well approximated by a modified 1D effective field theory, although we have recently shown in a numerically accurate time-dependent calculation [17] that spatial interference fringes of separated and recombined condensates in the exact many-body solution are much weaker than those predicted by the corresponding time-dependent mean field theory [16]. Although the Fermi-Bose mapping theorem [10,11] implies that all physical properties expressible in terms of spatial configurational probabilities are the same for the actual bosonic system and the fictitious “spinless fermion” system used for the mapping, the momentum distribution of the bosonic system, or more generally its occupation distribution over the relevant orbitals for a given geometry, is very different in the bosonic system. It is known [8,12,18] that for a spatially uniform system of hard core bosons in 1D, the momentum distribution is strongly peaked in the neighborhood of zero momentum, whereas that of the corresponding Fermi system is merely a filled Fermi sea. In the case of hard core bosons in a 1D harmonic trap, it has been an interesting question whether the system undergoes true BEC or merely an attenuated one such as that in the uniform system. Ketterle and Van Druten [19] have shown that true BEC occurs for a finite number of atoms in a 1D harmonic oscillator (HO) in the case of an *ideal* gas, but the behavior turns out to be different for the exact many-body solutions in the Tonks (1D) limit. The most fundamental definition of BEC and the condensate orbital is based on the large distance behavior of the one-particle reduced density matrix  $\rho_1(x, x')$ . If off-diagonal long-range order (ODLRO) is present and hence the largest eigenvalue of  $\rho_1$  is macroscopic (proportional to  $N$ ) then the system is said to exhibit true BEC and the

corresponding eigenfunction, the condensate orbital, plays the role of an order parameter [20,21]. Although the precise definition of ODLRO requires a thermodynamic limit not strictly applicable to mesoscopic traps, the GP approximation assumes from the start that ODLRO and macroscopic occupation of a single orbital are good approximations in a trap, so examination of this assumption is important. We have recently [22] used the Fermi-Bose mapping theorem to determine, for this case of 1D impenetrable bosons in a harmonic trap, the exact many-body ground state and its salient features, including the one-particle reduced density matrix and its eigenvalues (occupation number distribution function) and eigenfunctions (natural orbitals), as well as the momentum distribution function. We find that the largest eigenvalue of the one-particle density matrix is proportional to lower than the first power of  $N$ , as is the momentum distribution function at  $k = 0$ , so that the Tonks gas does not show true BEC.

In this paper we give an overview of our recent work on exact many-body quantum solutions for 1D Tonks gases. In particular, Secs. II and III describe the ground state and dynamic properties of Tonks gases, respectively. For the most part we investigate 1D Tonks gases assuming the conditions are satisfied for realizing them. In Sec. IV we examine the use of Bessel optical dipole traps for experimental realization of 1D Tonks gases.

## II. EXACT STATIONARY SOLUTIONS

We first describe the Fermi-Bose mapping method for obtaining exact solutions of the time-independent many-body Schrödinger equation in the Tonks limit (impenetrable point bosons) and its application to the spatially uniform case (no trap potential). This description is very brief and the original literature [10,11] should be consulted for details. Some salient features of the recent generalization to the harmonically trapped Tonks gas [22] are then described.

### A. Mapping theorem

Our basic model consists of  $N$  bosonic atoms at zero temperature moving in 1D ( $x$ ), the quantum motion in the other two spatial dimensions having been frozen out by tight transverse confinement via an atomic waveguide. The Schrödinger Hamiltonian is then assumed to have the structure:

$$\hat{H} = \sum_{j=1}^N -\frac{\hbar^2}{2m} \frac{\partial^2}{\partial x_j^2} + V(x_1, \dots, x_N), \quad (1)$$

where  $x_j$  is the one-dimensional position of the  $j$ th particle (atom) and  $V$  is symmetric (invariant) under permutations of the particles. The two-particle interaction potential is assumed to contain a hard core of 1D diameter  $a$ . This is conveniently treated as a constraint on allowed wave functions  $\psi(x_1, \dots, x_N)$ :

$$\psi = 0 \quad \text{if} \quad |x_j - x_k| < a \quad , \quad 1 \leq j < k \leq N, \quad (2)$$

rather than as an infinite contribution to  $V$ , which then consists of all other (finite) interactions and external potentials. Let  $\psi_F(x_1, \dots, x_N)$  be a fermionic solution of  $\hat{H}\psi = E\psi$  which

is antisymmetric under all particle pair exchanges  $x_j \leftrightarrow x_k$ , hence all permutations. One can consider  $\psi_F$  to be either the wave function of a fictitious system of “spinless fermions”, or else that of a system of real fermions whose spins are all aligned, as in magnetically trapped atomic vapor BECs. Define a “unit antisymmetric function” [10]

$$A(x_1, \dots, x_N) = \prod_{1 \leq j < k \leq N} \text{sgn}(x_k - x_j), \quad (3)$$

where  $\text{sgn}(x)$  is the algebraic sign of the coordinate difference  $x = x_k - x_j$ , i.e., it is  $+1(-1)$  if  $x > 0(x < 0)$ . For given antisymmetric  $\psi_F$ , define a bosonic wave function  $\psi_B$  by

$$\psi_B(x_1, \dots, x_N) = A(x_1, \dots, x_N)\psi_F(x_1, \dots, x_N) \quad (4)$$

which defines the Fermi-Bose mapping.  $\psi_B$  satisfies the hard core constraint (2) if  $\psi_F$  does, is totally symmetric (bosonic) under permutations, obeys the same boundary conditions as  $\psi_F$ , and  $\hat{H}\psi_B = E\psi_B$  follows from  $\hat{H}\psi_F = E\psi_F$  [10,11]. In the case of periodic boundary conditions (no trap potential, spatially uniform system) one must add the proviso that the boundary conditions are only preserved under the mapping if  $N$  is odd, but the case of even  $N$  is easily accommodated by imposing periodic boundary conditions on  $\psi_F$  but *antiperiodic* boundary conditions on  $\psi_B$ . For a trapped system the boundary condition that wave functions vanish at infinity is preserved for all  $N$ .

## B. Exact solution for untrapped bosons

The mapping theorem leads to explicit expressions for all many-body energy eigenstates and eigenvalues of a 1D scalar condensate (bosons all of the same spin) under the assumption that the only two-particle interaction is a zero-range hard core repulsion, represented by the  $a \rightarrow 0$  limit of the hard-core constraint. Such solutions were obtained in Sec. 3 of the original work [10] for periodic boundary conditions and no external potential. Such a situation could be realized experimentally, for example, by trapping the Tonks gas around the peak of a tight toroidal optical dipole trap formed using a red-detuned Laguerre-Gaussian laser beam [23]. In a system of 1D bosons with a hard-sphere interaction of diameter  $a$ , it is sufficient at low densities [8,9] to consider the case of impenetrable point particles, the zero-range limit  $a \rightarrow 0$ . Since wave functions of “spinless fermions” are antisymmetric under coordinate exchanges, their wave functions vanish automatically whenever any  $x_j = x_k$ , the constraint has no effect, and the corresponding fermionic ground state is the ground state of the *ideal* gas of fermions, a Slater determinant of the lowest  $N$  single-particle plane-wave orbitals. The exact many body ground state was found to be a pair product of Bijl-Jastrow form

$$\psi_0 = \text{const.} \prod_{i>j} |\sin[\pi L^{-1}(x_i - x_j)]|, \quad (5)$$

where  $L$  is the perimeter of the annular trap. In spite of the very long range of the individual pair correlation factors  $|\sin[\pi L^{-1}(x_i - x_j)]|$ , the pair distribution function  $D(x_{ij})$ , which is physically the joint probability density that if one particle is found at  $x_i$  a second will be found at  $x_j$ , was found to be of short range

$$D(x_{ij}) = 1 - \left( \frac{\sin(\pi \rho x_{ij})}{\pi \rho x_{ij}} \right)^2, \quad (6)$$

with  $\rho = N/L$  the linear number density of the system. Clearly,  $D(0) = 0$  which reflects the hard core nature of the two-particle interaction. By examination of the excited states the system was also found to support propagation of sound with speed  $c = \pi \hbar \rho / m$  [10].

### C. Harmonically trapped Tonks gas

Here we briefly review our recently-obtained exact solution for the many-body ground state of a harmonically trapped Tonks gas [22]. The Hamiltonian of  $N$  bosons in a 1D harmonic trap is

$$\hat{H} = \sum_{j=1}^N \left[ -\frac{\hbar^2}{2m} \frac{\partial^2}{\partial x_j^2} + \frac{1}{2} m \omega^2 x_j^2 \right]. \quad (7)$$

We again assume that the two-body interaction potential consists only of a hard core of negligible diameter  $a \rightarrow 0$ . It follows from the mapping theorem that the exact  $N$ -boson ground state  $\psi_{B0}$  is

$$\psi_{B0}(x_1, \dots, x_N) = |\psi_{F0}(x_1, \dots, x_N)|, \quad (8)$$

where  $\psi_{F0}$  is the ground state of a fictitious system of  $N$  spinless fermions with the same Hamiltonian and constraint. Since the hard-core interaction has no effect in the zero-range limit for fermions, whose wave functions already vanish at contact due to antisymmetry, it follows that the fermionic ground state is a Slater determinant of the lowest  $N$  single-particle eigenfunctions  $\phi_n$  of the harmonic oscillator (HO):

$$\psi_{F0}(x_1, \dots, x_N) = \frac{1}{\sqrt{N!}} \det_{(n,j)=(0,1)}^{(N-1,N)} \phi_n(x_j). \quad (9)$$

The HO orbitals are

$$\varphi_n(x) = \frac{1}{\pi^{1/4} x_{osc}^{1/2} \sqrt{2^n n!}} e^{-Q^2/2} H_n(Q) \quad (10)$$

with  $H_n(Q)$  the Hermite polynomials and  $Q = x/x_{osc}$ ,  $x_{osc} = \sqrt{\hbar/m\omega}$  being the ground state width of the harmonic trap for a single atom. By factoring the Gaussians out of the determinant and carrying out elementary row and column operations, one can cancel all terms in each  $H_n$  except the one of highest degree, with the result [24]

$$\begin{aligned} \det_{(n,j)=(0,1)}^{(N-1,N)} H_n(x_j) &= 2^{N(N-1)/2} \det_{(n,j)=(0,1)}^{(N-1,N)} (x_j)^n \\ &= 2^{N(N-1)/2} \prod_{1 \leq j < k \leq N} (x_k - x_j) \end{aligned} \quad (11)$$

Substitution into (6) then yields a simple but exact analytical expression of Bijl-Jastrow pair product form for the  $N$ -boson ground state:

$$\psi_{B0}(x_1, \dots, x_N) = C_N \left[ \prod_{i=1}^N e^{-Q_i^2/2} \right] \prod_{1 \leq j < k \leq N} |x_k - x_j| \quad (12)$$

with  $Q_i = x_i/x_{osc}$  and normalization constant

$$C_N = 2^{N(N-1)/4} \left( \frac{1}{x_{osc}} \right)^{N/2} \left[ N! \prod_{n=0}^{N-1} n! \sqrt{\pi} \right]^{-1/2}. \quad (13)$$

It is interesting to note the strong similarity between this exact 1D  $N$ -boson wave function and the famous Laughlin variational wave function of the 2D ground state for the quantized fractional Hall effect [25], as well as the closely-related wave functions for bosons with weak repulsive delta-function interactions in a harmonic trap in 2D found recently by Smith and Wilkin [26].

Both the single particle density and pair distribution function depend only on the absolute square of the many-body wave function, and since  $|\psi_{B0}|^2 = |\psi_{F0}|^2$  they reduce to standard ideal Fermi gas expressions. The single particle density, normalized to  $N$ , is

$$\rho(x) = N \int |\psi_{B0}(x, x_2, \dots, x_N)|^2 dx_2 \cdots dx_N = \sum_{n=0}^{N-1} |\varphi_n(x)|^2 \quad (14)$$

We shall not exhibit it here since it has recently been calculated by Kolomeisky *et al.* [16]; see also our recent discussion of the time-dependent case [17]. The pair distribution function, normalized to  $N(N-1)$ , is

$$\begin{aligned} D(x_1, x_2) &= N(N-1) \int |\psi_{B0}(x_1, \dots, x_N)|^2 dx_3 \cdots dx_N \\ &= \sum_{0 \leq n < n' \leq N-1} |\varphi_n(x_1)\varphi_{n'}(x_2) - \varphi_n(x_2)\varphi_{n'}(x_1)|^2 \end{aligned} \quad (15)$$

Noting that terms with  $n = n'$ , which vanish by antisymmetry, can be formally added to the summation (13), one can write

$$\begin{aligned} D(x_1, x_2) &= \rho(x_1)\rho(x_2) - |\Delta(x_1, x_2)|^2 \\ \Delta(x_1, x_2) &= \sum_{n=0}^{N-1} \varphi_n^*(x_1)\varphi_n(x_2) \end{aligned} \quad (16)$$

Although the Hermite polynomials have disappeared from the expression (10) for the many-body wave function, they reappear upon integrating  $|\psi_{B0}|^2$  over  $(N-1)$  coordinates to get the single particle density  $\rho(x)$  and over  $(N-2)$  to get the pair distribution function  $D(x_1, x_2)$ , and the expressions in terms of the HO orbitals  $\varphi_n$  are the most convenient for evaluation. Figure 1 shows a gray scale plot of the dimensionless pair distribution function  $x_{osc}^2 \cdot D(Q_1, Q_2)$  versus the normalized coordinates  $Q_{1,2} = x_{1,2}/x_{osc}$  for a)  $N = 2$ , b)  $N = 6$ , and c)  $N = 10$ . Some qualitative features of the pair distribution function are apparent: In the first place it follows either from the original expression (12) or from Eq. (14) that  $D(x_1, x_2)$  vanishes at contact  $x_1 = x_2$ , as it must because of impenetrability of the particles, and we see this to be true in Fig. 1. Furthermore, the correlation term  $\Delta(x_1, x_2)$  is a truncated closure sum and approaches the Dirac delta function  $\delta(x_1 - x_2)$  as  $N \rightarrow \infty$ , as is

to be expected since the healing length in a spatially uniform 1D hard core Bose gas varies inversely with particle number [14]. As a result the width of the null around the diagonal  $Q_1 = Q_2$  decreases with increasing  $N$ , and vanishes in the limit. Away from the diagonal along  $Q_2 = -Q_1$  the pair distribution function rises, exhibits modulations for  $N > 2$ , due to the oscillatory nature of the HO orbitals, before decreasing back to zero at large distances. For  $|x_1 - x_2|$  much larger than the healing length,  $D$  reduces to the uncorrelated density product  $\rho(x_1)\rho(x_2)$ , so the spatial extent of the pair distribution function is that of the density and varies as  $N^{1/2}$  [16].

The reduced single-particle density matrix with normalization  $\int \rho_1(x, x) dx = N$  is

$$\rho_1(x, x') = N \int \psi_{B0}(x, x_2, \dots, x_N) \psi_{B0}(x', x_2, \dots, x_N) dx_2 \dots dx_N \quad (17)$$

Although this multi-dimensional integral cannot be evaluated analytically, it can be evaluated numerically by Monte Carlo integration for not too large values of  $N$  (the computing time scales as  $N^4$ ). Figure 2 shows a gray scale plot of the dimensionless reduced single-particle density matrix  $x_{osc} \cdot \rho_1(Q, Q')$  versus the normalized coordinates  $Q$  and  $Q'$  for a)  $N = 2$ , b)  $N = 6$ , and c)  $N = 10$ . Along the diagonal  $\rho_1(Q, Q' = Q) = \rho(Q)$  reproduces the single-particle density [16]. The off-diagonal elements relate to ODLRO, and it is clear that as  $N$  increases the off-diagonal elements are decreasing, in contrast with the diagonal. This is an indication that ODLRO vanishes for a system of hard core bosons in a 1D HO in the thermodynamic limit, although at present only numerical evidence exists, there being no analytical proof generalizing the result of Lenard for the untrapped Tonks gas [12].

In a macroscopic system, the presence or absence of BEC is determined by the behavior of  $\rho_1(x, x')$  as  $|x - x'| \rightarrow \infty$ . Off-diagonal long-range order is present if the largest eigenvalue of  $\rho_1$  is macroscopic (proportional to  $N$ ), in which case the system exhibits BEC and the corresponding eigenfunction, the condensate orbital, plays the role of an order parameter [20,21]. Although this criterion is not strictly applicable to mesoscopic systems, if the largest eigenvalue of  $\rho_1$  is much larger than one then it is reasonable to expect that the system will exhibit some BEC-like coherence effects. Thus we examine here the spectrum of eigenvalues  $\lambda_j$  and associated eigenfunctions  $\phi_j(x)$  (“natural orbitals”) of  $\rho_1$ . Although natural orbitals are a much-used tool in theoretical chemistry, they have only recently been applied to mesoscopic atomic condensates [27]. The relevant eigensystem equation is

$$\int_{-\infty}^{\infty} \rho_1(x, x') \phi_j(x') dx' = \lambda_j \phi_j(x) \quad (18)$$

$\lambda_j$  represents the occupation of the orbital  $\phi_j$ , and one has  $\sum_j \lambda_j = N$ . Numerical evaluation of the integral by discretization yields a matrix eigensystem equation giving accurate numerical results for the largest eigenvalues and associated eigenvectors. We remark that for the corresponding problem of  $N$  free fermions in a 1D HO, in which case  $\rho_1(x, x')$  is evaluated using the fermion wave function  $\psi_{F0}(x_1, \dots, x_N)$ , the natural orbitals are simply the HO orbitals, and  $\lambda_j = 1, j = 0 \dots (N - 1)$ , all higher eigenvalues being zero (filled Fermi sea). However, the N-boson wave function is the modulus of the fermion wave function, and this leads to significant differences in the spectrum of natural orbitals and eigenvalues for the hard core Bose gas. In Fig. 3(a) we show a log-log plot of the fractional occupation of the lowest orbital  $f_0 = \lambda_0/N$  versus the total particle number  $N$  (solid line), along with a

best fit power-law  $f_0 \approx N^{-0.41}$  (dashed line). This is to be contrasted with the case of a spatially uniform system of hard core bosons for which  $f_0 \approx N^{-0.5}$  [12]. In both cases the fractional occupation decreases with increasing  $N$ , and thus does not correspond to a true condensate for which  $f_0 = 1$ . Nevertheless, the occupation of the lowest orbital may still be large,  $\lambda_0 \approx N^{0.59}$ , and is larger than the spatially uniform case  $\lambda_0 \approx N^{0.5}$ , so macroscopic quantum coherence effects reminiscent of BEC can still result [8,12–14,16,17]. Figure 3(b) shows the distribution of occupations  $\lambda_j$  versus orbital number  $j$  (the orbitals are ordered according to eigenvalue magnitude, the largest eigenvalue being  $j = 0$ ) for  $N = 2$  (circles),  $N = 6$  (stars), and  $N = 10$  (squares). This figure shows that as the lowest orbital occupation  $\lambda_0$  increases with increasing  $N$  so does the range of significantly occupied higher-order orbitals with  $j > 0$ . This means that the dominance of the lowest orbital decreases with increasing  $N$ , so singling out  $\phi_0(x)$  as a macroscopic wave function for the whole system becomes more problematic with increasing  $N$  [16,17].

Next we examine the momentum distribution for the trapped 1D Tonks gas. For a spatially uniform system (no trap) the natural orbitals are plane waves, so the occupation distribution of the natural orbitals is the same as the momentum distribution. Although this is not the case here due to the effect of the harmonic trap potential, the momentum distribution is still physically important. In terms of the boson annihilation and creation operators in position representation (quantized Bose field operators) the one-particle reduced density matrix is

$$\rho_1(x, x') = \langle \Psi_{B0} | \hat{\psi}^\dagger(x') \hat{\psi}(x) | \Psi_{B0} \rangle \quad (19)$$

The momentum distribution function  $n(k)$ , normalized to  $\int_{-\infty}^{\infty} n(k) dk = N$ , is  $n(k) = \langle \Psi_{B0} | \hat{a}^\dagger(k) \hat{a}(k) | \Psi_{B0} \rangle$  where  $\hat{a}(k)$  is the annihilation operator for a boson with momentum  $\hbar k$ . Then

$$n(k) = (2\pi)^{-1} \int_{-\infty}^{\infty} dx \int_{-\infty}^{\infty} dx' \rho_1(x, x') e^{-ik(x-x')} \quad (20)$$

The spectral representation of the density matrix then leads to  $n(k) = \sum_j \lambda_j |\mu_j(k)|^2$  where the  $\mu_j$  are Fourier transforms of the natural orbitals:  $\mu_j(k) = (2\pi)^{-1/2} \int_{-\infty}^{\infty} \phi_n(x) e^{-ikx} dx$ . Figure 4 shows the numerically calculated dimensionless momentum spectrum  $k_{osc} \cdot n(\kappa)$  versus normalized momentum  $\kappa = k/k_{osc}$ , with  $k_{osc} = 2\pi/x_{osc}$ , for a)  $N = 2$ , b)  $N = 6$ , and c)  $N = 10$ . The key features are that the momentum spectrum maintains the sharp peaked structure reminiscent of the spatially uniform case [8,12] for the 1D HO, and that the peak becomes sharper with increasing atom number  $N$ . This is to be expected since as the number of atoms increase the many-body repulsion causes the system to become more spatially uniform within the trap interior.

By way of contrast, for a 1D Fermi gas the corresponding momentum spectrum is a filled Fermi-sea, here rounded out by the trapping potential. In particular, the momentum distribution for the 1D trapped Fermi gas can be expressed as

$$n(k) = \sum_{j=1}^N |\mu_j(k)|^2, \quad (21)$$

Thus, the momentum spectrum provides a means of distinguishing between the 1D Fermi and Tonks gases. Figure 5 shows an example of the Tonks (dashed line) and Fermi gas (solid

line) momentum spectra for  $N = 10$  atoms in a harmonic trap, and the difference is clearly seen. Furthermore, the distinction only grows larger with increasing number of atoms, as the filled Fermi-sea broadens whereas the Tonks spectrum becomes narrower. In a recent paper we have devised a scheme to measure the momentum spectrum of trapped gases based on Raman outcoupling, and we refer the reader to our paper for details [28].

### III. DYNAMICAL SOLUTIONS

The Fermi-Bose mapping theorem is very easily generalized so as to yield exact solutions of the time-dependent many-body Schrödinger equation (TDMBSE) by noting that since the mapping function  $A(x_1, \dots, x_n)$  of Eq. (3) is independent of time, one can merely replace  $E\psi$  by  $i\hbar\partial\psi/\partial t$ , implying that the relationship of Eq. (4), with time arguments added to the Bose and Fermi wave functions, is valid for solutions of the TDMBSE. In the special case where the only interatomic interaction is that of hard cores of vanishing diameter, but external potentials including a trap potential as well as time-dependent fields may be present, the many-fermion solutions of the TDMBSE are Slater determinants of solutions of the *single particle* TDSE in the given external potential, and each many-boson solution is obtained by multiplying the corresponding determinant by the mapping function  $A(x_1, \dots, x_n)$ . Some salient features of our recently-obtained dynamical solutions for solitons in a ring geometry and for interference effects in a dynamically split, harmonically trapped Tonks gas will be described. The description will again be brief since details are available in the literature [14,17].

#### A. Dark solitons in a Tonks gas

Dark and gray solitons are a generic feature of the nonlinear Schrödinger equation with repulsive interactions, and several calculations of their dynamics based on the mean-field Gross-Pitaevskii (GP) equation have appeared [29–36], as well as experiments demonstrating their existence in atomic BECs [33,34]. Since the underlying *many-body* Schrödinger equation is linear, this raises the question of how observed solitonic behavior arises. Here this issue will be examined with the aid of exact many-body solutions for the Tonks gas. The model consists of a 1D hard-core Bose gas in a toroidal trap, or ring, with cross section so small that motion is essentially circumferential. The Fermi-Bose mapping is employed to generate exact solutions for this problem. We identify stationary solutions which reflect some properties of dark solitons from the GP theory when the ring is pierced at a point by an intense blue-detuned laser. We also present dynamical solutions when half of an initially homogeneous ring BEC is phase-imprinted via the light-shift potential of an applied laser, leading to gray soliton-like structures whose velocity depends on the imposed phase-shift [33,34]. Such structures are apparent for times less than the echo time  $\tau_e = L/c$ , with  $L$  the ring circumference and  $c$  the speed of sound in the BEC. On longer time scales the dynamics becomes very complex showing Talbot recurrences which are beyond the GP theory.

Consider  $N$  bosons in a tight toroidal trap, for example a toroidal optical dipole potential [23], and denote their 1D positions measured around the circumference by  $x_j$ . This is equivalent to the exactly-solved model [10] of  $N$  impenetrable point bosons in 1D with

wave functions satisfying periodic boundary conditions with period  $L$  equal to the torus circumference, and the fundamental periodicity cell may be chosen as  $-L/2 < x_j < L/2$ . However, the rotationally invariant quantum states of this problem do not reveal any dark soliton-like structures. To proceed we therefore consider the case that a blue-detuned laser field pierces the ring at  $x = 0$  by virtue of the associated repulsive dipole force: The light sheet then provides a reference position for the null of the dark soliton. Assume that the light sheet is so intense and narrow that it may be replaced by a constraint that the many-body wave function (hence the orbitals  $\phi_i$ ) must vanish whenever any  $x_j = 0$ . Then the appropriate orbitals  $\phi_i(x)$  are free-particle energy eigenstates vanishing at  $x = 0$  and periodic with period  $L$ . The complete orthonormal set of even-parity eigenstates  $\phi_n^{(+)}$  and odd-parity eigenstates  $\phi_n^{(-)}$  are

$$\begin{aligned}\phi_n^{(+)}(x) &= \sqrt{2/L} \sin[(2n-1)\pi|x|/L], \\ \phi_n^{(-)}(x) &= \sqrt{2/L} \sin(2n\pi x/L),\end{aligned}\tag{22}$$

with  $n$  running from 1 to  $\infty$ . The odd eigenstates are the same as those of free particles with no  $x = 0$  constraint, since these already vanish at  $x = 0$ . However, the even ones are strongly affected by the constraint, their cusp at  $x = 0$  being a result of the impenetrable light sheet at that point. If one bends a 1D box  $-L/2 < x < L/2$  with impenetrable walls into a ring, identifying the walls at  $\pm L/2$ , then those particle-in-a-box eigenfunctions which are even about the box center become identical with the  $\phi_n^{(+)}$ , and their cusp results from the nonzero slope of these functions at the walls. The  $N$ -fermion ground state is obtained by inserting the lowest  $N$  of these orbitals into a Slater determinant (filled Fermi sea). Since  $A^2 = 1$ , the one-particle density  $\rho(x)$  of the corresponding many-boson ground state given by Eq. (4) is the same as that of the  $N$ -fermion ground state. In the thermodynamic limit  $N \rightarrow \infty$ ,  $L \rightarrow \infty$ ,  $N/L \rightarrow \rho$  for fixed  $x$ ,  $\rho^{(\pm)}$ , one finds [14]

$$\rho(x) \sim \rho[1 - \sin(2\pi\rho x)/2\pi\rho].\tag{23}$$

$\rho(x)$  vanishes at  $x = 0$  and approaches the mean density  $\rho$  over a healing length  $L_h = 1/2\rho$  with damped spatial oscillations about its limiting value. Suppose next that the light-sheet is turned off at  $t = 0$  by removing the constraint that the wave function vanish at  $x = 0$ . The solution of the TDMBSB for the many-boson system is then still given by the mapping theorem, but the Slater determinant representing the corresponding many-fermion state has to be built from solutions of the time-dependent single-particle Schrödinger equation satisfying the initial conditions of Eq. (22). The odd-parity solutions are stationary in time since they already vanish at the position of the light sheet. The even-parity solutions are nontrivial, but are expressible as sums over the space-periodic, even-parity solutions of the time-independent free-particle Schrödinger equation [14]:

$$\phi_n^{(+)}(x, t) = \frac{2(2n-1)}{\pi} \sqrt{\frac{2}{L}} \sum_{p=0}^{\infty} \frac{(2 - \delta_{p0}) \cos(k_p x) e^{-i\omega_p t}}{(2n-1)^2 - 4p^2}\tag{24}$$

where  $\omega_p = \hbar k_p^2/2m$  and  $k_p = 2p\pi/L$ . The time-dependent density  $\rho(x, t)$  is then the sum of absolute squares of all  $N$  orbitals in the Fermi sea. It is found [14] that there are two important time scales: One is the Poincaré recurrence time  $\tau_r$ . Noting that  $\omega_p$  is proportional

to  $p^2$ , one finds that all terms in the sum are time-periodic with period  $\tau_r = mL^2/\pi\hbar$ , which is therefore the recurrence time for the density and in fact all properties of our model [13]. The other important time is the echo time  $\tau_e$ , the time for sound to make one circuit around the torus. Recalling that the speed of sound in this system is  $c = \pi\hbar\rho/m$  [10], one finds  $\tau_e = \tau_r/N$ . For  $t \ll \tau_e$  after the constraint is removed, the initial density develops sound waves that propagate around the ring, and that we examine below in the context of phase-imprinting. For  $t > \tau_e$  the evolution is very complex, but complete recurrences occur for times  $t = n\tau_r$  with fractional revivals in between.

Suppose next that the toroidal impenetrable point Bose gas is in its ground state for times  $t < 0$  (no light sheet obstacle in this case), and a phase-imprinting laser pulse is applied as a delta-function pulse over half the ring at  $t = 0$ . This is described by the Hamiltonian

$$\hat{H} = \sum_{j=1}^N \left[ -\frac{\hbar^2}{2m} \frac{\partial^2}{\partial x_j^2} - \hbar\Delta\theta\delta(t)S(x_j) \right] \quad (25)$$

where  $S(x) = \theta(L/4 - |x|)$ , i.e., unity for  $-L/4 < x < L/4$  and zero elsewhere. This is the technique used in recent experiments [33,34], here idealized to a delta-function in time and to sharp spatial edges. Before the pulse the most convenient free-particle orbitals in (5) are plane waves  $\phi_n(x) = \sqrt{(1/L)}e^{ik_nx}$  where  $k_n = 2n\pi/L$  and  $n = -n_F, -n_F + 1, \dots, n_F - 1, n_F$  with  $n_F = (N - 1)/2$ . Let  $\phi_n(x, t)$  be the solution of the corresponding single-particle TDSE reducing to the above  $\phi_n(x)$  just before the pulse. Then the solutions just after the pulse are  $\phi_n(x, 0+) = \phi_n(x)e^{iS(x)\Delta\theta}$ . The potential gradients at the pulse edges impart momentum kicks to the particles there which induce both compressional waves propagating at the speed,  $c$ , of sound and density dips (gray solitons) moving at speeds  $|v| < c$ . The expansion of  $\phi_n(x, t)$  in terms of the unperturbed plane waves is evaluated as

$$\begin{aligned} \phi_n(x, t) &= \frac{1}{2} \left( 1 + e^{i\Delta\theta} \right) - \frac{1 - e^{i\Delta\theta}}{\pi} \sum_{\ell=-\infty}^{\infty} \\ &\times \frac{(-1)^\ell \phi_{n-2\ell-1}(x) e^{-i\omega_{n-2\ell-1}t}}{2\ell + 1} \end{aligned} \quad (26)$$

and the time-dependent density is the sum of the absolute squares of the lowest  $N$  of these. Figure 6 shows numerical simulations for  $N = 51$ ,  $t/\tau_e = 0.051$ , and  $\Delta\theta = \pi$  (solid line), and  $\Delta\theta = 0.5\pi$  (dashed line): due to symmetry we show only half of the ring  $-L/2 < x < 0$ , the phase shift being imposed at  $x = -L/4$ . Considering times short compared to the echo time means that the corresponding results are not very sensitive to the periodic boundary conditions, and also therefore apply to a linear geometry. The initial density profile is flat with a value  $\rho_0 L = 51$ . For both phase shifts two distinct maxima are seen, which travel at close to the speed of sound  $c$ , and two distinct minima, which are analogous to gray solitons and travel at velocities  $|v|/c < 1$ . In addition, there are also high wavevector oscillations which radiate at velocities greater than  $c$ , analogous to precursors in electromagnetic wave propagation in a medium. In the case of a phase shift  $\Delta\theta = \pi$ , the density is symmetric about  $x = -L/4$ , whereas for a phase-shift other than a multiple of  $\pi$  the evolution is not symmetric, see the dashed line where the global minimum moves to the right in response to the phase shift. In Fig. 7 we plot the calculated velocity of the global density minimum relative to the speed of sound for a variety of phase shifts  $\Delta\theta$ . The basic trend is that larger

phase-shift means lower velocity, in qualitative agreement with recent experiments [33,34], but there is a sharp velocity peak at  $\Delta\theta \approx 0.83\pi$ : This peak results from the cross-over between two local minima in the density. These general features, the generation of gray solitons and density waves, agree with those of the GP theory, but here arise out of the exact many-body calculation.

A detailed comparison between our results and current experiments is not possible as they do not conform to the conditions for a 1D system. However, some estimates are in order to set the appropriate time scales: If we consider  $^{87}\text{Rb}$  with a ring of circumference  $L = 100 \mu\text{m}$ , and a high transverse trapping frequency  $\omega_{\perp} = 2\pi \times 10^5 \text{ Hz}$ , then we are limited to atom numbers  $N < 300$  [8], so these are small condensates. We then obtain  $\tau_r = 4.6 \text{ s}$ , and  $\tau_e = 90 \text{ ms}$  for  $N = 51$ . Finally, we remark that since our approach relied on the mapping between the strongly-interacting Bose system and a non-interacting “spinless Fermi gas” model, this suggests that dark and gray solitons should also manifest themselves in the density for the 1D Fermi system. Although real fermions have spin, the interactions used here to generate solitons were spin-independent.

## B. Suppression of interference in a dynamically split and recombined Tonks gas

Mean-field theory (MFT) has proven remarkably successful at predicting both the static and dynamic behavior of Bose-Einstein condensates (BECs) in weakly-interacting atomic vapors [37], including the ground state properties [38,39], the spectrum of collective excitations [40,41], four-wave mixing [42,43], matter-wave solitons [44,45], and interference between BECs [46–49]. The basic notion underlying MFT is of a macroscopic wave function [20,21], or order parameter, which defines the spatial mode into which a significant fraction of the atoms condense below the critical temperature. The macroscopic wave function typically obeys a nonlinear Schrödinger equation (NLSE), the Gross-Pitaevskii equation, and is most suitable for dilute Bose gases. However, the success of MFT is not assured in all cases. For example, in one-dimension (1D) a spatially homogeneous ideal gas in its many-body ground state exhibits complete BEC into the lowest single-particle state, but no BEC at any nonzero temperature. Furthermore, previous exact analysis [10,11] of a spatially uniform Tonks gas by one of us (MG) and its extension by Lenard [12] and Vaidya and Tracey [18] have shown that in the many-body ground state the occupation of the lowest single-particle state is of order  $\sqrt{N}$  where  $N$  is the total number of atoms, in contrast to  $N$  for usual BEC, and similar behavior, but with a slightly larger exponent, occurs in the harmonically trapped Tonks gas [22]. We have recently shown that mean-field theory breaks down in the analysis of the dynamics of 1D atom clouds, in that it predicts interference effects that are absent in the exact theory [50]. Kolomeisky *et al.* [16] have proposed a nonlinear Schrödinger equation (NLSE) with a quartic nonlinearity to extend the usual mean-field theory for 1D atom clouds. For a harmonic trap the ground-state density profiles from their theory show excellent agreement with the exact many-body results (see Fig. 1 of their paper). The key question, then, is whether this extended NLSE can be used in all circumstances. To address this issue we examine the problem of a 1D atomic cloud in the ground state of a harmonic trap that is split by a blue-detuned laser and recombined, both using an exact many-body treatment based on the Fermi-Bose mapping and the approximate NLSE: the NLSE predicts interference whereas the exact analysis does not.

Consider a Tonks gas which is initially in its  $N$ -body ground state in a harmonic trap [22]. A central Gaussian repulsive potential simulating a blue-detuned laser field is turned on quasi-adiabatically at time  $t = 0$  to split the initial state. After some time  $t_{pot}$  both the harmonic trap and repulsive potential are turned off and the two split components allowed to recombine: this is an interference experiment of the cool, cut, interfere variety previously discussed [47]. The external potential is taken of the specific form

$$V(x, t) = \frac{1}{2}m\omega^2x^2 + V_B \sin\left(\frac{\pi t}{2t_{pot}}\right)e^{-x^2/w^2}, \quad (27)$$

and  $V = 0$  for  $t > t_{pot}$ . Figure 8 shows an illustrative example for  $N = 10$  with a repulsive potential of height  $V_B = 20\hbar\omega$ , and width  $w = 3x_0$ , with  $x_0 = \sqrt{\hbar/2m\omega}$  the ground state harmonic oscillator width, and  $\omega t_{pot} = 3$ . This figure shows a gray scale plot of the single-particle density  $\rho_N(x, t) = \sum_{i=1}^N |\phi_i(x, t)|^2$  of the  $N$ -boson system as functions of  $\omega t$  (horizontal axis) and position  $x/x_0$  (vertical axis), with white being the highest density. The potential height was chosen such that  $V_B > \mu = \hbar\omega(N - 1/2)$ , where  $\mu$  is the chemical potential of the  $N$ -particle oscillator ground state [16], noting that the top of the  $N$ -particle Fermi sea is at  $n = N - 1$ . As expected, as the repulsive potential turns on it splits the initial ground state into two separated components. Upon release at  $t = t_{pot}$  the two components expand and subsequently recombine. What is noteworthy is that although there is some modulation upon recombination there are no strong interference fringes indicative of the interference provisionally expected for bosons: this was a generic finding from our simulations irrespective of the time scale on which the repulsive potential was turned on [47,48]. In contrast, the density  $|\phi_i(x, t)|^2$  for each individual orbital  $i = 1, \dots, N$  can show strong fringes, but with a different period in each case. Thus, the minimal interference is a result of washing out of the individual interferences by summing over  $N$  orbitals. Thus, the remnant of any interference fringes decreases with increasing  $N$  and vanishes in the thermodynamic limit. Physically, it makes sense that the interference fringes are all but absent since the Fermi-Bose mapping shows that in this 1D limit the system of bosons acts effectively like a system of free fermions insofar as effects expressible only in terms of  $|\psi_B|^2$  are concerned, so interference is not expected [51]. The lack of interference is therefore a signature of the Fermi-Bose duality that occurs in 1D systems of impenetrable particles [10].

We next turn to the mean-field description proposed by Kolomeisky *et al.* [16] for low-dimensional systems. In particular, they introduce an order parameter  $\Phi(x, t)$ , normalized to the number of particles  $N$ , for such systems. Using energy functional arguments they deduce the following NLSE with quartic nonlinearity for a 1D system of impenetrable bosons:

$$i\hbar \frac{\partial \Phi}{\partial t} = \left[ -\frac{\hbar^2}{2m} \frac{\partial^2}{\partial x^2} + V(x, t) + \frac{(\pi\hbar)^2}{2m} |\Phi|^4 \right] \Phi. \quad (28)$$

Our goal is to compare the predictions of this NLSE for the same cool, cut, interfere simulation in Figure 8, with the initial condition  $\Phi(x, 0) = \sqrt{\rho_N(x, 0)}$  corresponding to the exact many-body solution, all other parameters being equal. Figure 9 shows the corresponding gray-scale plot of the density  $\rho(x, t) = |\Phi(x, t)|^2$ , and two features are apparent: First, during the splitting phase when the repulsive potential is on there is very good overall agreement between the exact many-body theory and the NLSE prediction. Second, when the split

components are released and recombine they produce pronounced interference fringes, in contrast to the exact theory. Indeed, this interference in the MFT is to be expected on the basis of previous theoretical work [46], even though a quartic (rather than quadratic) nonlinearity is employed here. Thus the MFT cannot accurately capture the time-dependent dynamics in all situations.

#### IV. BESSEL OPTICAL DIPOLE TRAPS FOR TONKS GASES

So far we have assumed that conditions are satisfied for the Tonks limit. However, previous analysis by Olshanii [8] and Petrov et al. [9] show that there are stringent requirements on the temperature, transverse confinement, and linear atom number density to approach the Tonks limit. Clearly, what is needed first of all it to create a thin cigar shaped atomic trap so that the transverse mode becomes frozen and the atomic motion becomes essentially 1D. Recent experimental developments suggest that Tonks gases may be realizable in magnetic atom waveguides [1,3,4], and Bongs et al. [15] have proposed a hybrid trap composed of optical dipole trap formed with a first-order LG beam combined with magnetic longitudinal trapping. Here we examine the use of Bessel optical dipole traps as an all-optical means to realize 1D Tonks gases.

Ideal Bessel beams are solutions of the free-space wave equation which propagate with unchanging beam profile along the propagation axis which we take as  $x$  in cylindrical coordinates  $(r, \theta, x)$ . The electric field of a monochromatic, linearly polarized ideal Bessel beam of order  $\ell$  and frequency  $\omega_L$  is [52]

$$\mathbf{E}(r, \theta, x, t) = \frac{\epsilon}{2} \left( E_0 J_\ell(k_r r) e^{i(k_x x + \ell\theta - \omega_L t)} + c.c. \right), \quad (29)$$

where  $E_0$  is a scale electric field value,  $J_\ell$  is the  $\ell$ th order Bessel function,  $\ell > 0$  is the azimuthal mode number which we take as positive for simplicity in notation, and  $k_r$  and  $k_x$  are the radial and longitudinal wavevectors such that  $k^2 = k_r^2 + k_x^2$  with  $k = \omega_L/c = 2\pi/\lambda_L$ . The zeroth-order solution  $J_0$  has a central maximum surrounded by concentric rings of roughly equal power while the higher-order solutions  $J_\ell$  have zero on-axis intensity also with concentric rings.

The utility of Bessel beams for optical dipole traps lies in the fact that they can produce very elongated, and hence low aspect ratio quasi-1D traps. In practice, of course, one cannot produce an ideal Bessel optical beams as it carries infinite power. However, using axiconal optics finite power approximations to Bessel beams can be produced which can propagate over significant distances. The basic scheme is illustrated in Figure 10 where an incident Laguerre-Gaussian beam of azimuthal mode index  $\ell$  is transformed into a Bessel beam of the same order. The interested reader is referred to our recent paper [53] for details, but for an incident Gaussian beam on the axiconal optics the resulting zero-order Bessel beam intensity profile past the axicon is

$$I_0(r, x) \approx 2\pi k_r w_0 \left( \frac{P_0}{\pi w_0^2/2} \right) \left( \frac{x}{x_{max}} \right) \exp(-2x^2/x_{max}^2) J_0^2(k_r r), \quad (30)$$

where  $w_0$  is the input spot size,  $P_0$  the input power,  $k_r = k(n-1)\gamma$ ,  $n$  and  $\gamma$  are the index and opening angle of the axicon, and  $x_{max} = kw_0/k_r$  which gives the longitudinal extent of

the Bessel beam. This intensity profile of the Bessel optical beam is readily converted to an effective dipole potential

$$\begin{aligned} V(r, x) &= \frac{\hbar\Gamma^2}{8\Delta} \left( \frac{I(r, x)}{I_{Sat}} \right) \\ &= \frac{1}{2} M\Omega_{r0}^2 \left( r^2 + \lambda^2(x - x_{peak})^2 \right), \end{aligned} \quad (31)$$

with  $\Delta = \omega_L - \omega_A$  the laser detuning from the optical transition frequency  $\omega_A$ ,  $\Gamma$  the natural linewidth of the optical transition,  $I_{Sat}$  is the resonant saturation intensity, and  $I(\mathbf{r}, t) = \frac{1}{2}\epsilon_0 c |E(r, z)|^2$ . For a red-detuned laser the potential is negative and the atoms are attracted to the regions of high intensity, whereas for a blue-detuned laser the atoms are repelled into the low field regions. Here for a red-detuned laser we have approximated the Bessel optical dipole potential by a parabolic potential near the axis under conditions of tight confinement, where  $x_{peak} = x_{max}/2$  is the longitudinal position of the peak of the Bessel beam, and

$$\Omega_{r0}^2 = \exp(-1/2) \frac{\hbar\Gamma^2}{4|\Delta|} \frac{P_0}{M I_{Sat}} \frac{k}{x_{max}} k_r^2, \quad \lambda = \frac{2\sqrt{2}}{k w_0} = \frac{2.83}{k_r x_{max}}. \quad (32)$$

A red-detuned ( $\Delta < 0$ )  $J_0$  optical dipole potential therefore provides confinement in both the radial and longitudinal directions. Here  $\Omega_{r0}$  is the radial oscillation frequency with corresponding ground state oscillator width  $w_{r0} = \sqrt{\hbar/M\Omega_{r0}}$ , and  $\lambda$  is the ratio between the longitudinal and radial trap frequencies  $\Omega_{x0}/\Omega_{r0} = \lambda$  [38,54,55], which also determines the aspect ratio between the radial and longitudinal ground state widths  $w_{r0}/w_{x0} = \sqrt{\lambda}$  (in the absence of many-body repulsion).

Petrov *et al.* [9] have theoretically studied the diagram of state for a one-dimensional gas of trapped bosons, assuming  $\lambda \ll 1$ , and found that a true BEC, or at least a quasi-condensate, with concomitant macroscopic occupation of a single state, is only attained for high enough particle numbers  $N > N_*$  with

$$N_* = \left( \frac{M g w_{x0}}{\hbar^2} \right)^2 = \left( 2 \left( \frac{a}{w_{r0}} \right) \left( \frac{w_{x0}}{w_{r0}} \right) \right)^2. \quad (33)$$

For  $N < N_*$  and temperatures  $T < N\hbar\Omega_{x0}$ , one obtains a Tonks gas of impenetrable bosons for which hard core repulsion between the bosonic atoms prevents them from penetrating through each other in the one-dimensional system, and the system acquires properties reminiscent of a one-dimensional system of fermionic atoms. A highly elongated Bessel beam discussed, say with parameters  $\lambda_L = 1064$  nm,  $P_0 = 5$  W,  $x_{max} = 10$  cm,  $1/k_r = 1.25$   $\mu$ m, would be an ideal candidate for the experimental realization of a Tonks gas. The low aspect ratio  $\lambda = 3.5 \times 10^{-4}$  and tight radial confinement  $w_{r0} = 82$  nm result in a high upper boundary  $N_*$  for the particle number of the Tonks gas. For the commonly used  $^{87}\text{Rb}$  isotope with a scattering length  $a = 5$  nm one finds  $N_* = 420$ . Although this is still a fairly low value it should be possible to experimentally realize a small  $^{87}\text{Rb}$  Tonks gas. However, more promising would be the use of the  $^{85}\text{Rb}$  isotope, where a Feshbach resonance can be used to tune the normally negative scattering length to positive values of several hundred nanometers magnitude [56]. As  $N_*$  is proportional to the square of the scattering length

even a moderate increase to  $a = 50$  nm would make it possible to create a larger Tonks gas, with say  $N = 2000$  atoms, which should be easily detectable.

The Bessel beam trap offers some advantages compared to alternative suggested approaches using magnetic waveguides [1,3,4] and a hybrid magnetic-optical trap [15]. Firstly, it involves only a very simple *all-optical* system for which the aspect ratio of the trap may be controlled simply by varying the Gaussian spot size incident on the axicon. More specifically, being all-optical, it does not involve material surfaces as in magnetic waveguides, which can cause matter-wave decoherence [57,58]. Furthermore, it allows for the possibility of trapping multiple magnetic sublevels and the investigation of multi-component Tonks gases, which would not be possible in the hybrid magnetic-optical trap of Bongs *et al.* [15].

## V. SUMMARY AND CONCLUSIONS

In this paper we have given an overview of our work on the quantum dynamics of 1D trapped Tonks gases. In particular, we hope to have shown that Tonks gases display a rich variety of behaviors that are worthy of experimental investigation. The Fermi-Bose mapping approach to solving for the 1D Tonks shows that many features are shared between the Tonks gas of impenetrable bosons and a 1D gas of non-interacting fermions: they have the same ground state energies and density profiles, and neither shows true BEC. However, the Tonks and Fermi gases differ markedly in their momentum spectra, and we have devised a scheme to measure this difference [28]. Furthermore, we have shown that the 1D Tonks gas can show dark soliton-like solutions which are typically associated with solutions of the mean-field Gross-Pitaevskii equation. This is so in spite of the fact that mean-field theory greatly overestimates the coherence properties of the Tonks gas, as we demonstrated in our simulations of split and recombined Tonks gases.

Our work presented here shows that Tonks gases have some degree of coherence but much less than a true BEC, and this may have implications for proposed atomic interferometers employing high density, eg. atom laser, sources. In particular, strong transverse confinement is desirable in atomic interferometers to avoid multi-transverse mode effects, and at the same time one would like to keep the atomic density down to avoid many-body shifts, but these are exactly the requirements for the Tonks limit! Therefore it is very important to study the BEC-Tonks transition [59] and its effect on the performance of atom interferometers. We hope that our work is a first step in this direction.

This work was supported at the University of Arizona by Office of Naval Research grant N00014-99-1-0806 and also the US Army Research office. We thank Joe Triscari for collaborations on the ground state properties of the Tonks gas, and the work on Bessel optical dipole traps was conducted in collaboration with J. Arlt and K. Dholakia from St. Andrews University, Scotland, and J. Soneson at the University of Arizona.

## REFERENCES

- [1] M. Key *et al.*, Phys. Rev. Lett. **84**, 1371 (2000).
- [2] D. Müller *et al.*, Phys. Rev. Lett. **83**, 5194 (1999).
- [3] N.H. Dekker *et al.*, Phys. Rev. Lett. **84**, 1124 (2000).
- [4] J.H. Thywissen, R.M. Westervelt, and M. Prentiss, Phys. Rev. Lett. **83**, 3762 (1999).
- [5] E.A. Hinds, M.G. Boshier, and I.G. Hughes, Phys. Rev. Lett. **80**, 645 (1998).
- [6] *Atom Interferometry*, ed. P.R. Berman (Academic Press, Boston, 1997).
- [7] J. Schmiedmayer, Eur. Phys. J. D **4**, 57 (1998).
- [8] M. Olshanii, Phys. Rev. Lett. **81**, 938 (1998).
- [9] D. S. Petrov, G. V. Shlyapnikov, and J. T. M. Walraven, Phys. Rev. Lett. **85**, 3745 (2000).
- [10] M. Girardeau, J. Math. Phys. **1**, 516 (1960).
- [11] M.D. Girardeau, Phys. Rev. **139**, B500 (1965). See particularly Secs. 2, 3, and 6.
- [12] A. Lenard, J. Math. Phys. **7**, 1268 (1966).
- [13] A. G. Rojo, G. L. Cohen, and P. R. Berman, Phys. Rev. A **60**, 1482 (1999).
- [14] M.D. Girardeau and E.M. Wright, Phys. Rev. Lett. **84**, 5691 (2000).
- [15] K. Bongs *et al.*, Phys. Rev. A **63**, 031602(R) (2001).
- [16] E. B. Kolomeisky *et al.* Phys. Rev. Lett. **85**, 1146 (2000).
- [17] M.D. Girardeau and E.M. Wright, Phys. Rev. Lett. **84**, 5239 (2000).
- [18] H.G. Vaidya and C.A. Tracey, Phys. Rev. Lett. **42**, 3 (1979).
- [19] W. Ketterle and N. J. Van Druten, Phys. Rev. A **54**, 656 (1996).
- [20] O. Penrose and L. Onsager, Phys. Rev. **104**, 576 (1956).
- [21] C.N. Yang, Rev. Mod. Phys. **34**, 694 (1962).
- [22] M.D. Girardeau, E.M. Wright, and J.M. Triscari, Phys. Rev. A **63**, 033601 (2001).
- [23] E.M. Wright, J. Arlt, and K. Dholakia, Phys. Rev. A **63**, 013608 (2000).
- [24] A.C. Aitken, *Determinants and Matrices* (Oliver and Boyd, Edinburgh and London, 1951), p. 112.
- [25] R.B. Laughlin, Phys. Rev. Lett. **50**, 1395 (1983).
- [26] R.A. Smith and N.K. Wilkin, Phys. Rev. A **62**, 061602 (2000).
- [27] J. L. DuBois and H. R. Glyde, Phys. Rev. A **023602**, 2000 (.)
- [28] M.D. Girardeau and E.M. Wright, cond-mat/0012365 (2000).
- [29] W.P. Reinhardt and C.W. Clark, J. Phys. B: At. Mol. Opt. Phys. **30**, L785 (1997).
- [30] R. Dum *et al.*, Phys. Rev. Lett. **80**, 2972 (1998).
- [31] T.F. Scott, R.J. Ballagh, and K. Burnett, J. Phys. B: At. Mol. Opt. Phys. **31**, L329 (1998).
- [32] A.D. Jackson, G.M. Kavoulakis, and C.J. Pethick, Phys. Rev. A **58**, 2417 (1998).
- [33] S. Burger *et al.*, Phys. Rev. Lett. **83**, 5198 (1999).
- [34] J. Denshlag *et al.* Science **287**, 97 (1999).
- [35] A.E. Muryshev *et al.*, Phys. Rev. A **60**, R2665 (1999).
- [36] Th. Busch and J.R. Anglin, Phys. Rev. Lett. **84**, 2298 (2000).
- [37] For a recent review see F. Dalfovo *et al.*, Rev. Mod. Phys. **71**, 463 (1999).
- [38] G. Baym and C. J. Pethick, Phys. Rev. Lett. **76**, 6 (1996).
- [39] Y. Kagan, G. V. Shlapnikov, and J. T. M. Walraven, Phys. Rev. Lett. **76**, 2670 (1996).
- [40] M. Edwards *et al.*, Phys. Rev. Lett. **77**, 1671 (1996).
- [41] S. Stringari, Phys. Rev. Lett. **77**, 2360 (1996).

- [42] E. V. Goldstein, K. Plättner, and P. Meystre, *Quantum. Semiclass. Opt.* **7**, 743 (1995).
- [43] L. Deng *et al.*, *Science* **398**, 218 (1999).
- [44] S. A. Morgan, R. J. Ballagh, and K. Burnett, *Phys. Rev. A* **55**, 4338 (1997).
- [45] W.P. Reinhardt and C.W. Clark, *J. Phys. B: At. Mol. Opt. Phys.* **30**, L785 (1997).
- [46] M. Naraschewski *et al.*, *Phys. Rev. A* **54**, 2185 (1996).
- [47] J. Javanainen and M. Wilkens, *Phys. Rev. Lett.* **78**, 4675 (1997); *ibid.* **81**, 1345 (1998).
- [48] A. J. Legget and F. Sols, *Phys. Rev. Lett.* **81**, 1344 (1998).
- [49] E. M. Wright *et al.*, *Phys. Rev. A* **56**, 591 (1997).
- [50] M.D. Girardeau and E.M. Wright, *Phys. Rev. Lett.* **84**, 5239 (2000).
- [51] K. E. Cahill and R. J. Glauber *Phys. Rev. A* **59**, 1538 (1999).
- [52] J. Durnin, J. J. Miceli, and J. H. Eberly, *Phys. Rev. Lett.* **58**, 1499 (1987).
- [53] J. Arlt *et al.*, to be published in *Phys. Rev. A* (2001).
- [54] V. M. Perez-Garcia *et al.*, *Phys. Rev. A* **57**, 3837 (1998).
- [55] Y. S. Kivshar and T. J. Alexander, cond-mat/9905048 (1999).
- [56] S. L. Cornish *et al.*, *Phys. Rev. Lett.* **85**, 1795 (2000).
- [57] C. Henkel and M. Wilkens, *Europhys. Lett.* **47**, 414 (1999).
- [58] C. Henkel, S. Poetting, and M. Wilkens, *Appl. Phys. B* **69**, 379 (1999).
- [59] V. Dunjko, V. Lorent, and M. Olshanii, cond-mat/0103085 (2001).

## FIGURES

FIG. 1. Gray-scale plots of the dimensionless pair distribution function  $x_{osc}^2 \cdot D(Q_1, Q_2)$  as a function of the dimensionless coordinates  $Q_1$  and  $Q_2$ , for a)  $N = 2$ , b)  $N = 6$ , and c)  $N = 10$ .

FIG. 2. Gray-scale plots of the dimensionless reduced density matrix  $x_{osc} \cdot \rho_1(Q, Q')$  as a function of the dimensionless coordinates  $Q$  and  $Q'$ , for a)  $N = 2$ , b)  $N = 6$ , and c)  $N = 10$ .

FIG. 3. Occupation of the natural orbitals: a) fraction of atoms in the lowest orbital  $f_0 = \lambda_0/N$  versus  $N$ , and b)  $\lambda_j$  versus orbital number  $j$  for  $N = 2$  (circles),  $N = 6$  (stars), and  $N = 10$  (squares).

FIG. 4. Dimensionless momentum distribution  $k_{osc} \cdot n(\kappa)$  versus normalized momentum  $\kappa = k/k_{osc}$  for a)  $N = 2$ , b)  $N = 6$ , and c)  $N = 10$ .

FIG. 5. Angular cross section versus angle  $\sin(\theta) \approx \theta$  for  $N = 10$ . The dashed line is for the 1D gas of impenetrable bosons and the solid line is for the corresponding system of non-interacting fermions

FIG. 6. Scaled density  $\rho(x, t)L$  versus scaled position around the ring  $x/L$  for  $N = 51$ ,  $t/\tau_e = 0.051$ , and  $\Delta\theta = \pi$  (solid line), and  $\Delta\theta = 0.5\pi$  (dashed line). Due to symmetry we show only half of the ring  $-L/2 < x < 0$ , the phase-jump being imposed at  $x = -L/4$ .

FIG. 7. Dark soliton velocity  $|v|/c$  scaled to the speed of sound  $c$  as a function of phase-shift  $\Delta\theta/\pi$  for  $N = 51$ .

FIG. 8. Exact many-body theory simulation of the cool, cut, interfere scenario. The figure shows a gray-scale plot of the particle density  $\rho_N(x, t)$  as a function of  $\omega t$  (horizontal axis) and position  $x/x_0$  (vertical axis), with white being the highest density, for  $N = 10$ ,  $V_B = 20\hbar\omega$ ,  $w = 3x_0$ , and  $\omega t_{pot} = 3$ .

FIG. 9. Mean-field theory simulation of the cool, cut, interfere scenario. The figure shows a gray-scale plot of the particle density  $\rho(x, t) = |\Phi(x, t)|^2$  as a function of  $\omega t$  (horizontal axis) and position  $x/x_0$  (vertical axis). Parameters are the same as Fig. 7.

FIG. 10. Illuminating an axicon with a LG mode of order  $\ell$  produces a Bessel beam of the same order within the shaded region.

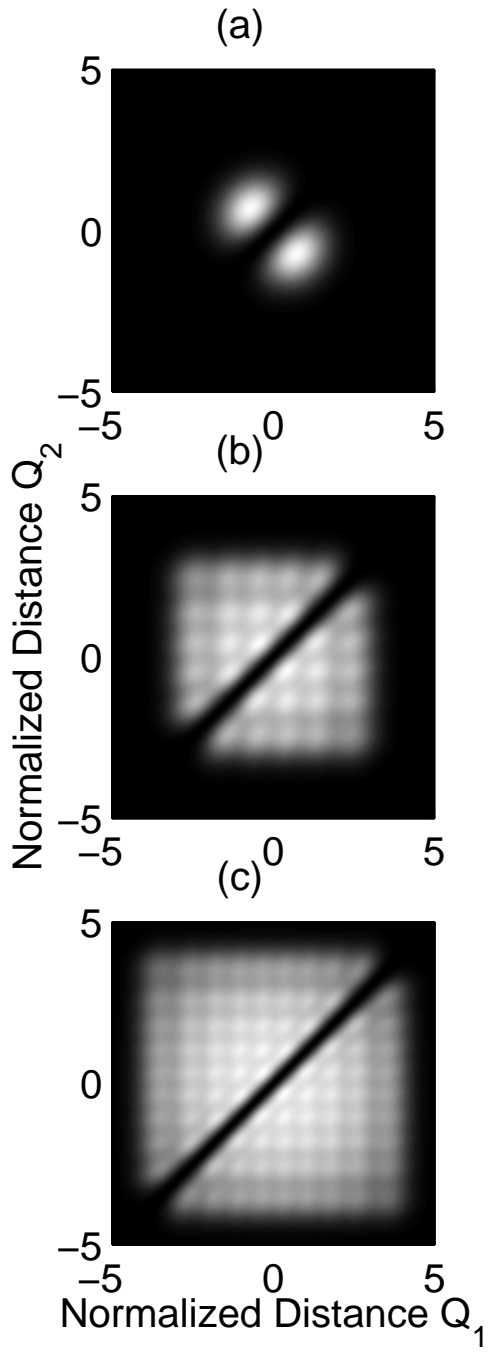


Figure 1

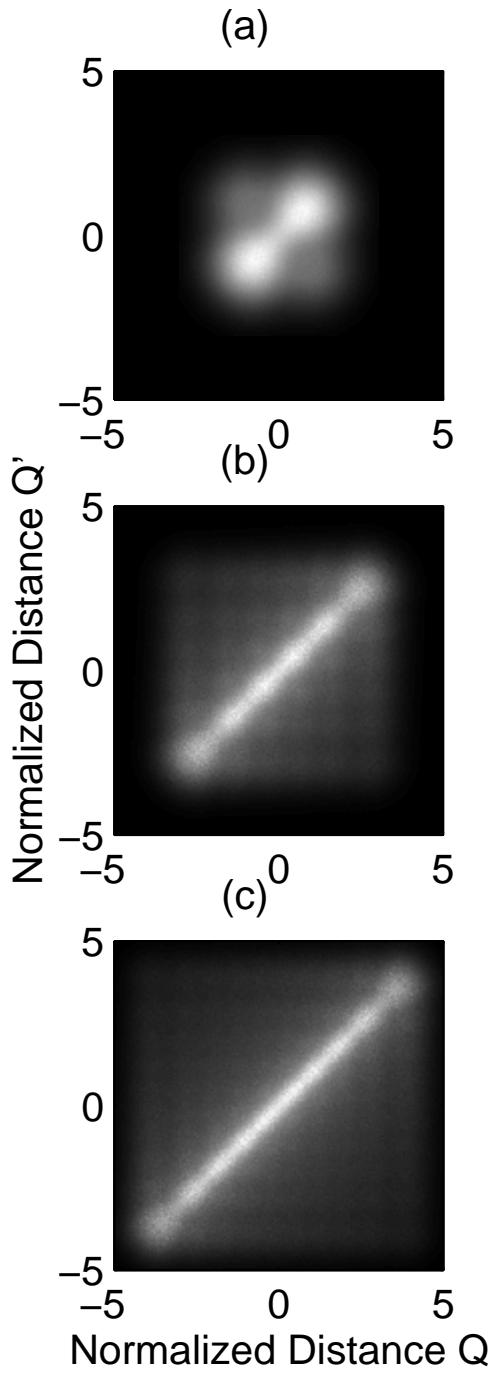


Figure 2

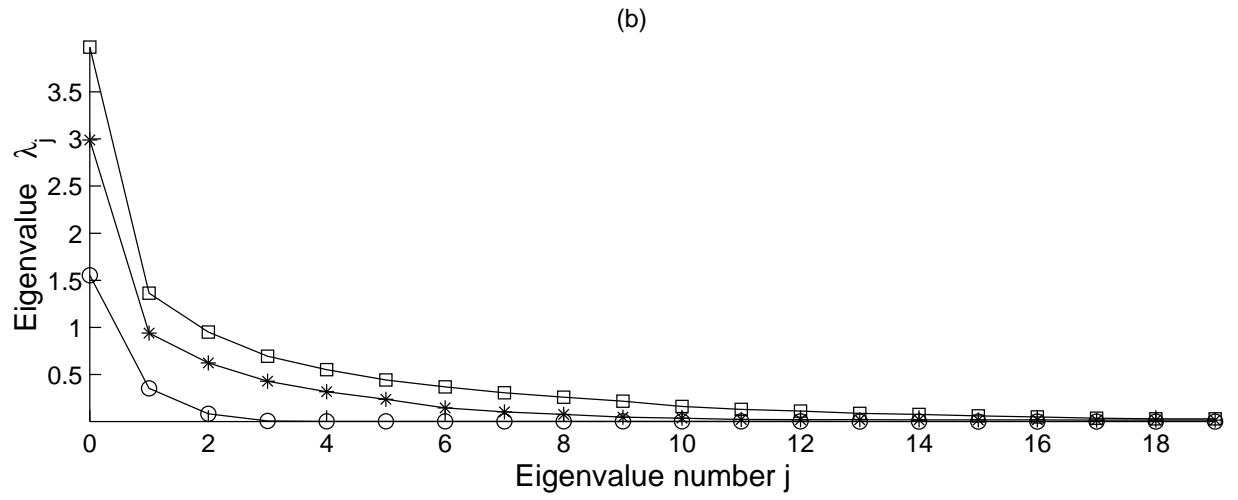
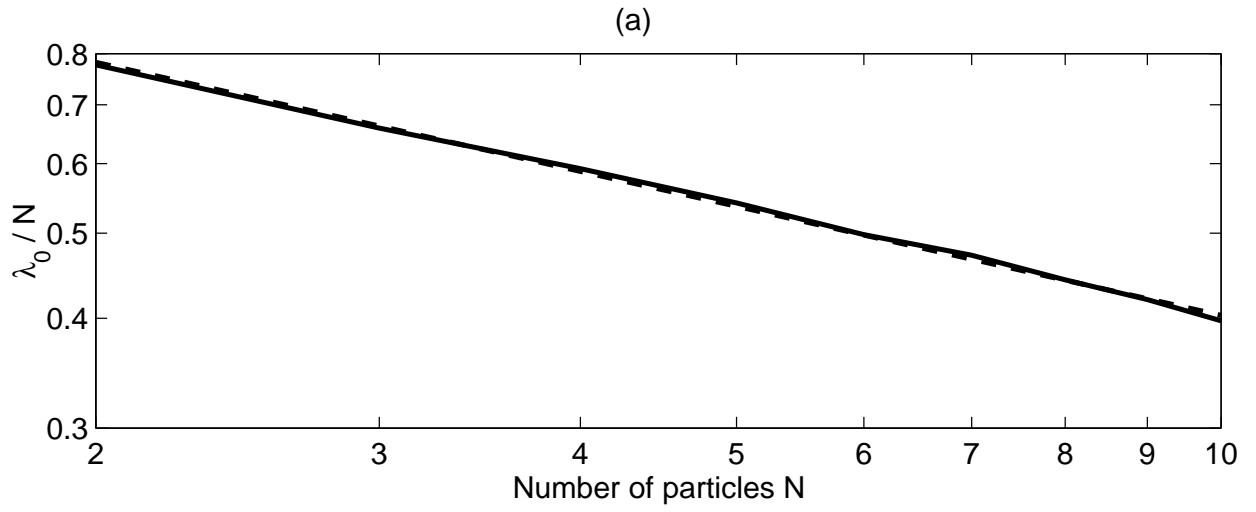


Figure 3

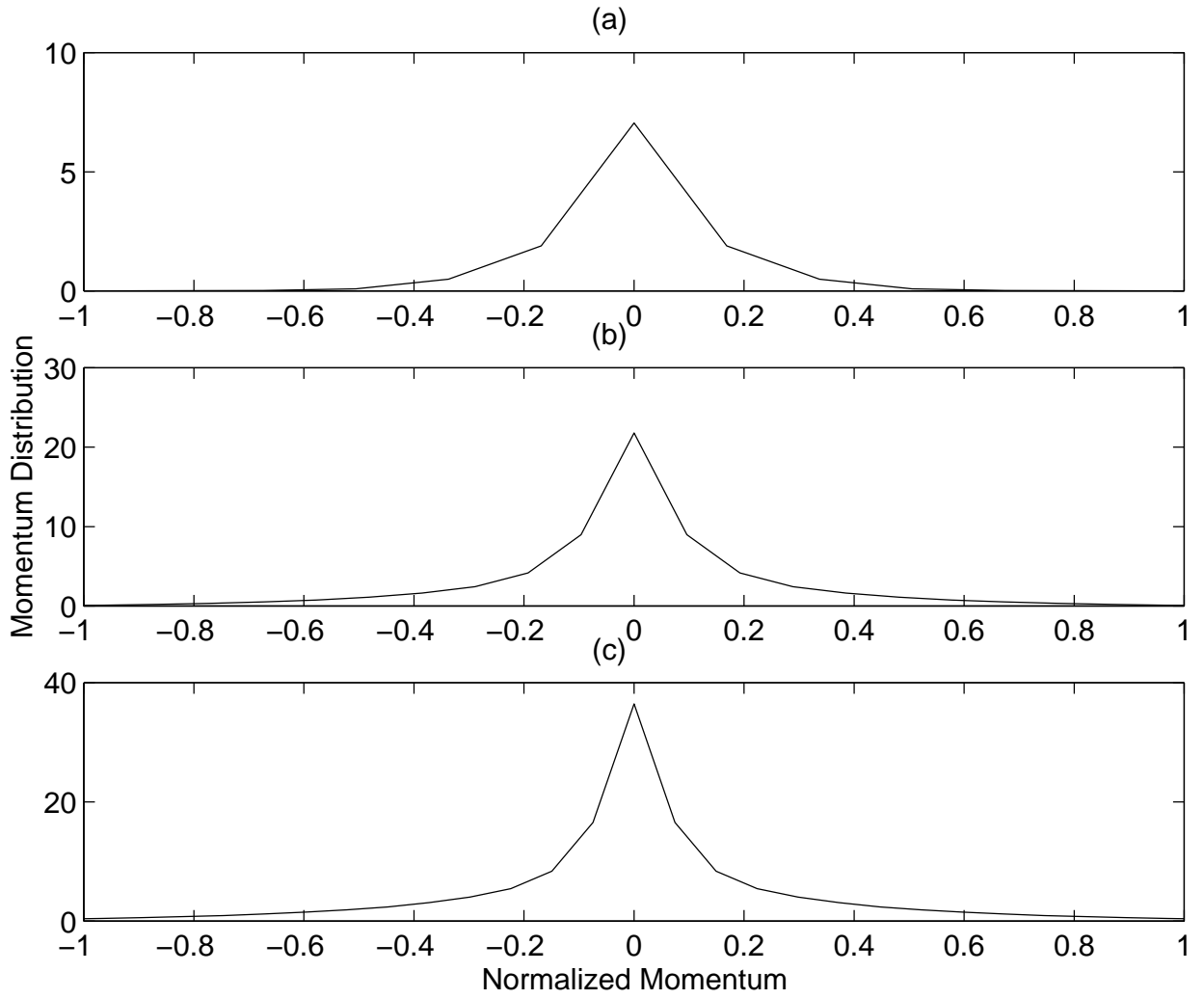


Figure 4

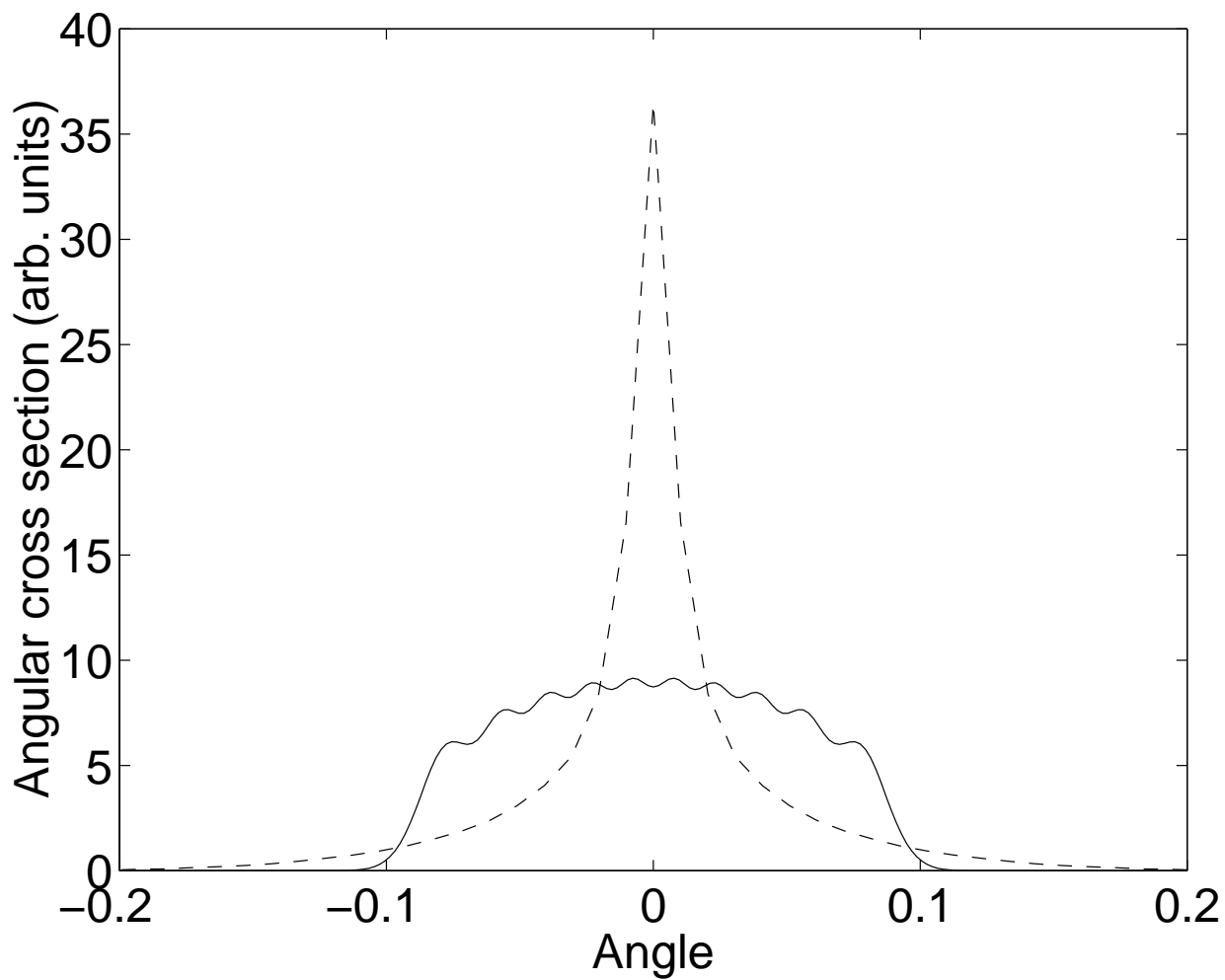


Figure 5

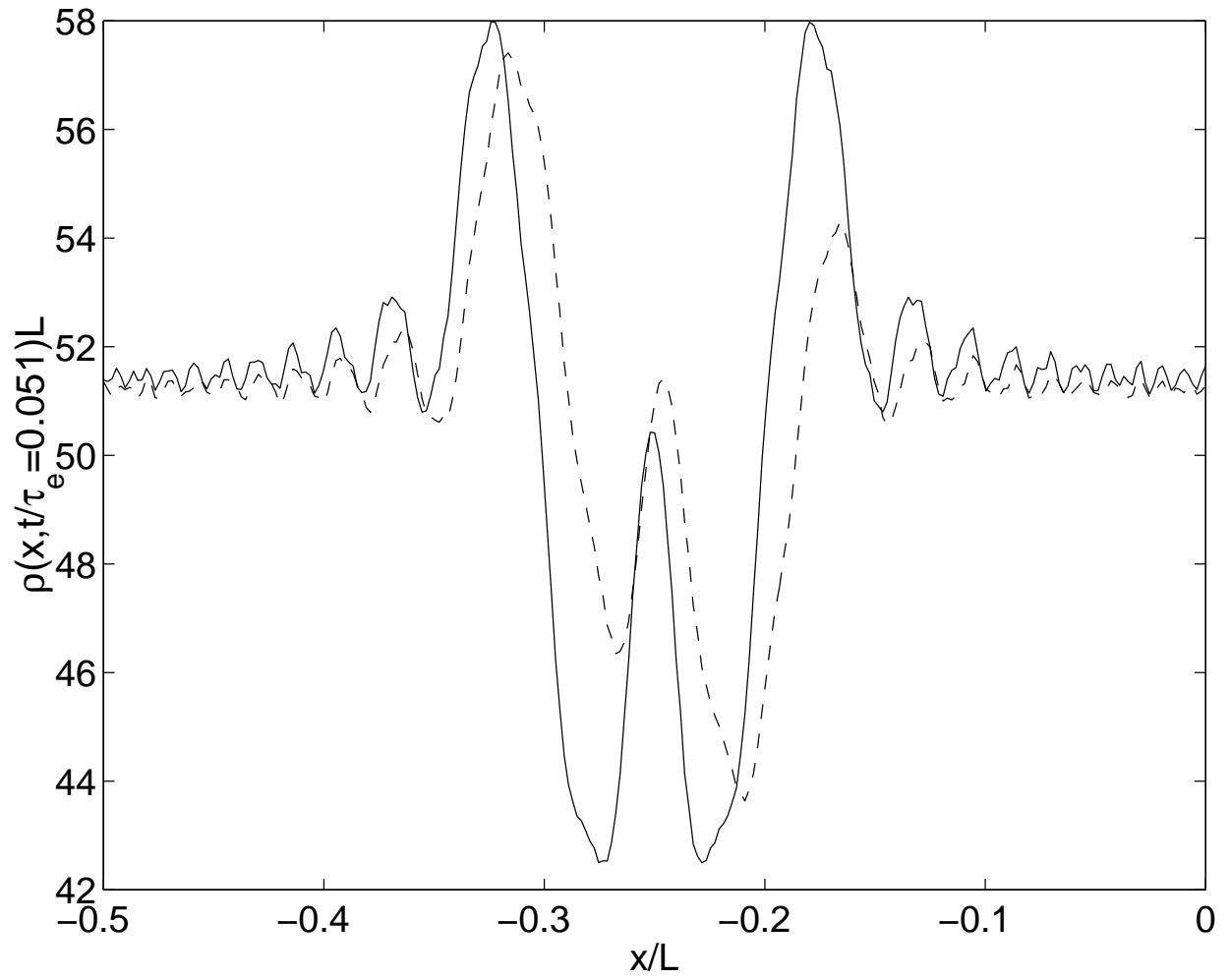


Figure 6

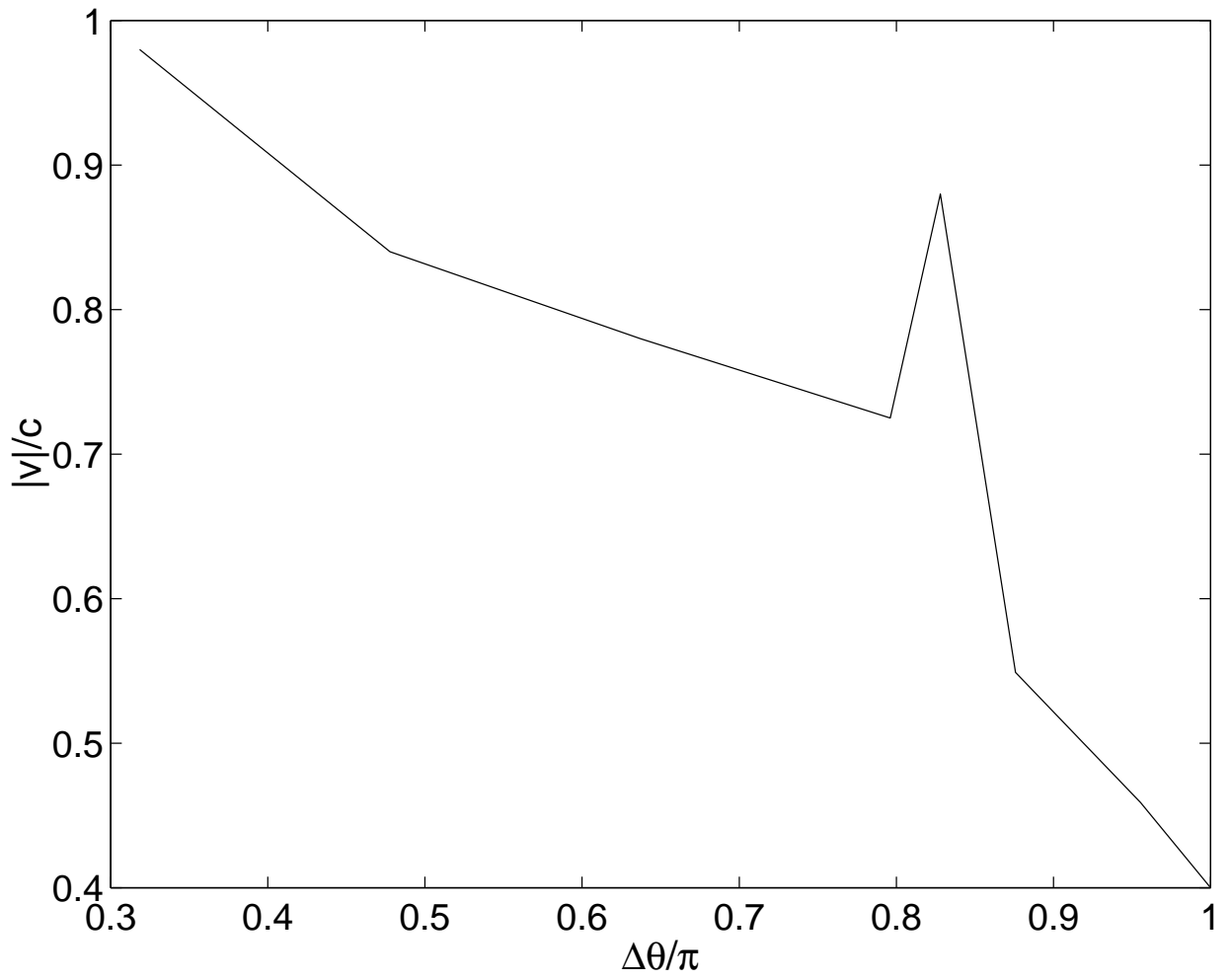


Figure 7

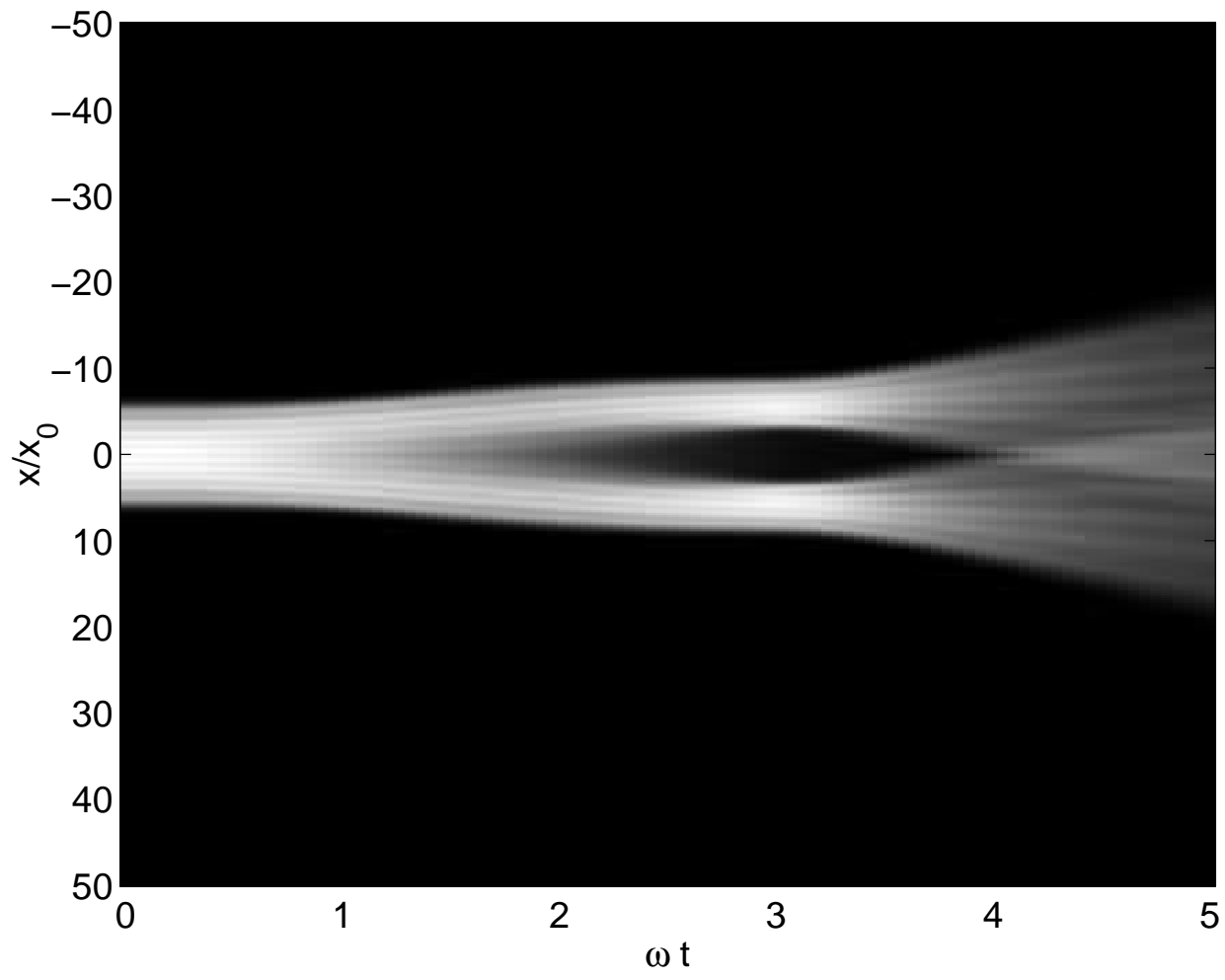


Figure 8

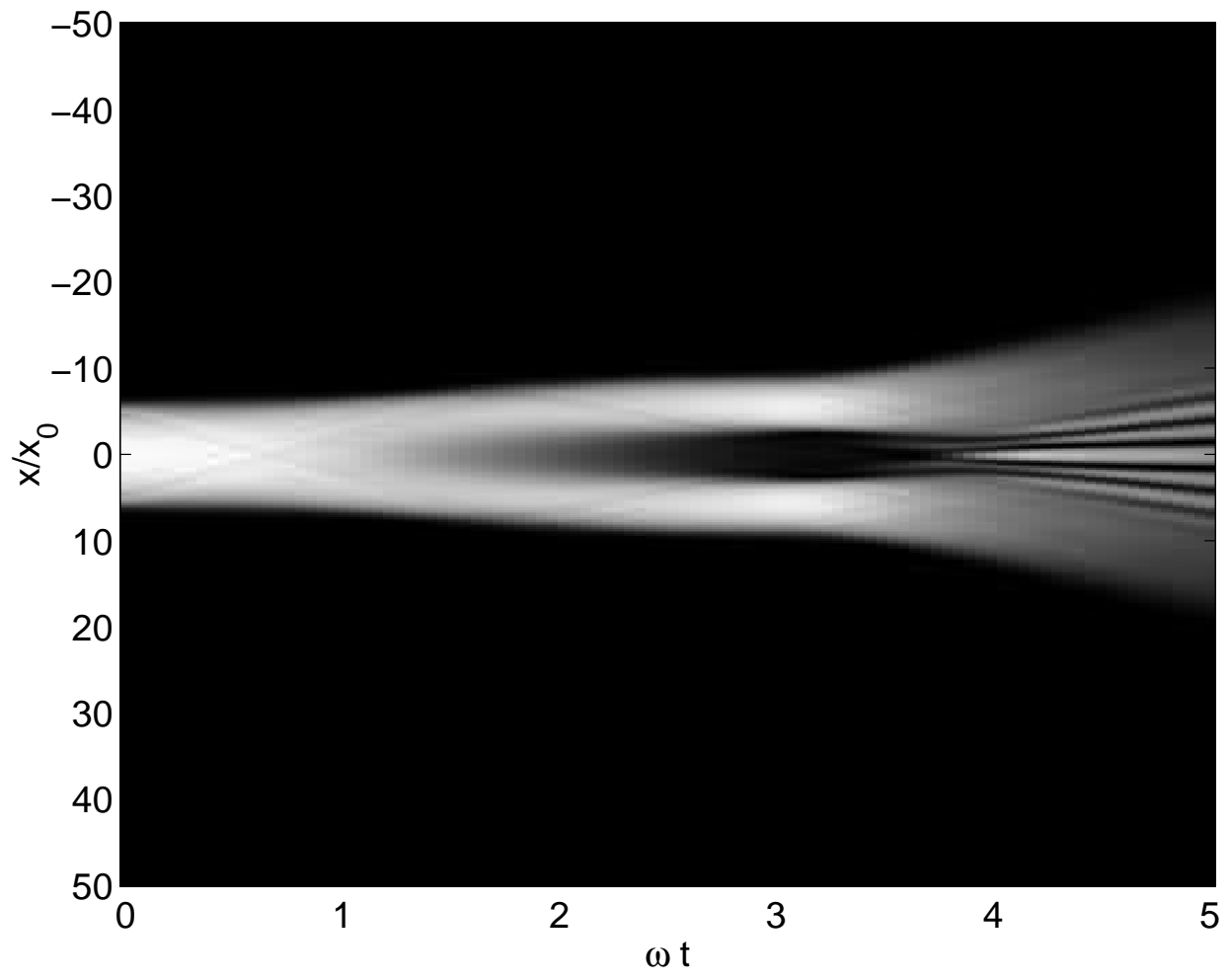


Figure 9

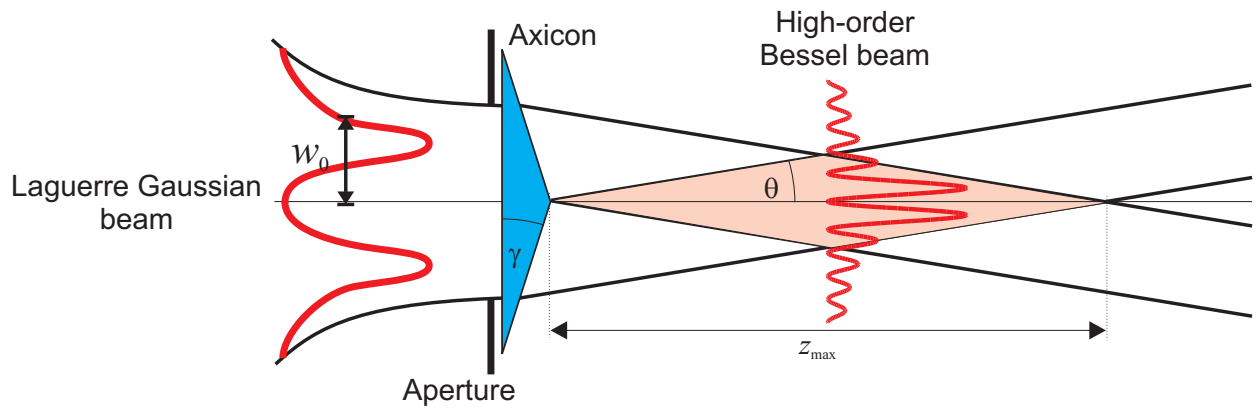


Figure 10